CAMBRIDGE
UNIVERSITY PRESS

Article

Constraints on the Equations of State of stiff anisotropic minerals: rutile, and the implications for rutile elastic barometry

Gabriele Zaffiro, Ross J. Angel* and Matteo Alvaro

Department of Earth and Environmental Sciences, University of Pavia, Via A. Ferrata, 1 I-27100, Pavia, Italy

Abstract

We present an assessment of the thermo-elastic behaviour of rutile based on X-ray diffraction data and direct elastic measurements available in the literature. The data confirms that the quasi-harmonic approximation is not valid for rutile because rutile exhibits substantial anisotropic thermal pressure, meaning that the unit-cell parameters change significantly along isochors. Simultaneous fitting of both the diffraction and elasticity data yields parameters of $K_{TR0} = 205.14(15)$ GPa, $K_{SR0} = 207.30(14)$ GPa, $K'_{TR0} = 6.9(4)$ in a 3rd-order Birch-Murnaghan Equation of State for compression, $\alpha_{V0} = 2.526(16) \times 10^{-5}$ K^{-1}, Einstein temperature $\theta_E = 328(12)$ K, Anderson-Grüneisen parameter $\delta_T = 7.6(6)$, with a fixed thermal Grüneisen parameter $\gamma = 1.4$ to describe the thermal expansion and variation of bulk modulus with temperature at room pressure. This Equation of State fits all of the available data up to 7.3 GPa at room temperature, and up to 1100 K at room pressure within its uncertainties. We also present a series of formulations and a simple protocol to obtain thermodynamically consistent Equations of State for the volume and the unit-cell parameters for stiff materials, such as rutile. In combination with published data for garnets, the Equation of State for rutile indicates that rutile inclusions trapped inside garnets in metamorphic rocks should exhibit negative residual pressures when measured at room conditions.

Introduction

Rutile (tetragonal, space group P4$_2$/mnm) is one of the polymorphs of TiO$_2$. It is a common accessory mineral in metamorphic rocks such as gneisses and schists and it is the primary titanium-bearing phase in eclogites (e.g. Meinhold, 2010). Mei *et al.* (2014) summarised all of the density functional theory (DFT) studies of the TiO$_2$ polymorphs and provided an equilibrium phase diagram that appears to be fairly consistent with experimental data available in the literature. This suggests that anatase is the thermodynamically stable phase at room conditions, whereas rutile becomes the thermodynamically stable phase above 1200 K and therefore it is metastable up to 1200 K at atmospheric pressure. The occurrence of rutile inclusions in metamorphic rocks indicates that rutile is the thermodynamically stable phase at metamorphic conditions. The high-pressure polymorphs of rutile were studied extensively with X-ray diffraction (XRD) experiments in diamond-anvil cells (e.g. Dubrovinskaia *et al.*, 2001; Al-Khatatbeh *et al.*, 2009). The first transition of rutile upon compression is to a phase with an α-PbO$_2$ type structure called TiO$_2$ II. The pressure for this transition ranges from 2.6 GPa to 34 GPa (McQueen *et al.*, 1967; Nicol and Fong, 1971; Al'tshuler *et al.*, 1973; Mammone *et al.*, 1980; Syono *et al.*, 1987; Arashi, 1992). XRD experiments (Sato, 1977; Ming and Manghnani, 1979; Hazen and Finger, 1981; Kudoh and Takeda,

1986; Gerward and Staun Olsen, 1997) are however in agreement with each other in demonstrating that rutile shows no transition below 12 GPa at room temperature. However, Kojitani *et al.* (2018) calculated from thermodynamic properties that the equilibrium phase boundary between rutile and TiO$_2$ II passes through room conditions, which implies that rutile is metastable at any pressure at room temperature. Therefore, the thermodynamic stability of rutile remains unclear and we restrict our analysis to pressures of less than 7.3 GPa, and temperatures less than 1100 K, under which conditions rutile at least appears to be kinetically stable and does not normally transform to other TiO$_2$ polymorphs.

Rutile is commonly formed during prograde metamorphism by reactions that also generate garnet, for example (e.g. Meinhold, 2010; Zack and Kooijman, 2017):

$$\text{anorthite} + \text{quartz} + 2 \text{ ilmenite} = \text{garnet(Gr1Alm2)} + 2 \text{ rutile}$$

$$\text{Al}_2\text{SiO}_5 + 2 \text{ quartz} + 3 \text{ ilmenite} = \text{almandine} + 3 \text{ rutile}$$
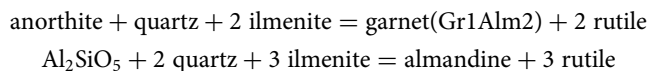
When rutile is formed together with garnet, or when it is already present in the protolith, it can be trapped as inclusions in garnet. Whereas the distribution of Ti between rutile and other minerals, such as quartz, is commonly used as a geothermometer for metamorphic rocks (e.g. Zack and Kooijman, 2017), the potential for using rutile inclusions in garnets as an elastic geobarometer has not yet been evaluated. Elastic geobarometry is based on the evidence that minerals trapped as inclusions within other host minerals can develop non-lithostatic pressures on exhumation as a result of the differences between the thermo-elastic properties of the host

and inclusion phases (e.g. Angel *et al.*, 2015). With modern Equations of State (EoS) and elasticity data of the mineral phases, the entrapment conditions of host-inclusion systems can be derived from the residual pressure measured in the inclusions at room conditions (e.g. Zhang, 1998; Kohn, 2014; Angel *et al.*, 2017). In this study, we evaluate for the first time whether rutile inclusions in garnets can be used for host-inclusion geobarometry by critically examining its EoS. The difficulty is that rutile is a very stiff material and the changes in its unit-cell volume and cell parameters are small over its *P–T* range of stability. Thus, it is not possible to determine reliable EoS parameters simply by performing conventional refinements to individual *P–V* or *P–V–T* datasets. Therefore, we make use of the fact that the variation with *P* and *T* of the bulk modulus of a crystal is determined by the same EoS parameters that define the variation of the unit-cell volume. We re-analyse all of the available literature for the variation of unit-cell parameters and elastic moduli of rutile with *P* and *T*, to obtain an internally-consistent dataset. We then determine the EoS parameters by a simultaneous fit to the compression, expansion and elasticity data. In doing so we discuss the criteria for obtaining self-consistency between the fits to the volumes and the cell parameters, which provide further constraints on the EoS parameters and also a 'recipe book' for the refinement of the EoS of other anisotropic stiff materials.

Data

The elastic properties of rutile have been studied extensively as a function of both pressure and temperature by means of different experimental techniques and computational studies. Mei *et al.* (2014) demonstrated that the elastic properties of rutile from DFT simulations are strongly dependent upon the choice of exchange–correlation functional used, with their own calculations showing a total spread of 60 GPa in the value of the isothermal Reuss bulk modulus, $K_{TR} = -V \left(\frac{\partial P}{\partial V} \right)_T$. Given the difficulties of extending computer simulations to finite temperatures, in part because of the limitations of the quasi-harmonic approximation that we discuss below, we therefore only include experimental data in this analysis. Compressional data available in the literature obtained by various diffraction methods at room temperature extend to 10.6 GPa but exhibit considerable data scatter in the volume measurements above 7.3 GPa (Fig. 1), and similar behaviour in the values of the unit-cell parameters. We therefore restricted our dataset to the more consistent studies below 7.3 GPa (Table 1). Because the excluded data are not inconsistent (within their large uncertainties) with the data used in the reported EoS fits, their inclusion in the fits makes no significant difference to the refined parameters but only increases their estimated uncertainties.

The available data for volume (and cell parameter) variation with temperature at room pressure is much more consistent (Fig. 2*a*), with the exception of the data of Wang *et al.* (2013) and the data point of Meagher and Lager (1979) at 1173 K which were excluded from the current analysis because they are inconsistent with the remaining data (Fig 2*a*). The reasons for these inconsistencies are not obvious from the published information. Of special importance for constraining both the appropriate thermal expansion model and its coefficients are the precise data collected below room temperature by optical interferometry (Kirby, 1967) and by neutron powder diffraction (Burdett *et al.*, 1987). To the best of our knowledge there are no measurements of the volume of rutile at simultaneous high *P* and *T*.
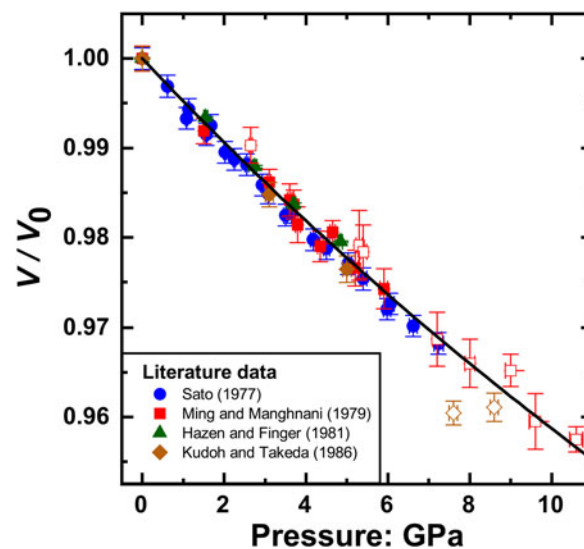

Fig. 1. *P–V* data of rutile taken from the literature. The open symbols are the data excluded from the current analysis. The full symbols are the selected data fitted with the final EoS (solid line) with the parameters given in Table 2.

The full elastic tensor of rutile as a function of temperature up to 1800 K was determined by Isaak *et al.* (1998) using the rectangular parallelepiped resonance (RPR) method, from which the variation of the adiabatic Reuss bulk $K_{SR} = -V \left(\frac{\partial P}{\partial V} \right)_S$ and linear moduli $M_{1SR} = M_{2SR} = -a \left(\frac{\partial P}{\partial a} \right)_S$ and $M_{3SR} = -c \left(\frac{\partial P}{\partial c} \right)_S$ can be obtained. Unfortunately, the low-temperature determinations of the elastic tensor of rutile by Manghnani *et al.* (1972) are incomplete and no moduli can be obtained from them, and the results of Fritz (1974) are only reported as pressure and temperature derivatives. We are therefore only able to use the interpolated values for the elastic tensor components up to 0.75 GPa that are reported in Manghnani (1969) in addition to data from Isaak *et al.* (1998). Fritz (1974) shows that all of these earlier studies are in reasonable agreement with each other with the exception of the first derivative of M_{3S}. We use the pressure derivatives reported by Fritz (1974), as an additional constraint when fitting the unit-cell parameters because his values for the pressure derivatives of the linear moduli are in better agreement with the XRD data reported in the literature than the linear moduli that can be obtained from the elastic moduli reported by Manghnani (1969).

In most solids, the thermal expansion coefficient increases or remains constant at high temperatures (e.g. Anderson, 1995). However, at high temperatures above ~1100 K, the measured unit-cell volumes of rutile deviate towards smaller values than would be expected by extrapolation from lower temperatures, implying that rutile is denser than expected (Fig. 2*a*). In agreement with this observation, $\left(\frac{\partial K_{SR}}{\partial T} \right)_{P=0}$ becomes less negative above 1100 K than at lower temperatures (Fig. 2*b* and Isaak *et al.*, 1998) meaning that rutile is stiffer than expected at high temperatures. This behaviour is in part due to the anomalous stiffening of the acoustic phonons driven by hybridisation of electrons between the Ti and O atoms (Lan *et al.*, 2015) and causes a change in the atomic-scale expansion mechanism within the rutile structure at high temperatures (see Sugiyama and Takeuchi, 1991). The effects of partial oxidation in some

Table 1. Data used to determine elastic parameters for rutile.

Source	Data type	P range (GPa)	T range (K)	Ndata
Sato (1977)	Powder XRD	0–7.24	Ambient	20
Ming and Manghnani (1979)	Powder XRD	0–5.9	Ambient	9
Hazen and Finger (1981)	Single-crystal XRD	0–4.84	Ambient	4
Kudoh and Takeda (1986)	Single-crystal XRD	0–5.0	Ambient	2
Manghnani (1969)	Elastic moduli from ultrasonic wave velocities	0–0.75	Ambient	4
Kirby (1967)	Length measurements by interferometry	Ambient	100–700	12
Rao *et al.* (1970)	Powder XRD	Ambient	298–918	14
Meagher and Lager (1979)	Single-crystal XRD	Ambient	298–873	2
Burdett *et al.* (1987)	Neutron powder diffraction	Ambient	15	1
Sugiyama and Takeuchi (1991)	Single-crystal XRD	Ambient	298–943	3
Hummer *et al.* (2007)	Powder XRD	Ambient	298–563	15
Henderson *et al.* (2009)	Neutron powder diffraction	Ambient	298–1065	12
Isaak *et al.* (1998)	Elastic moduli from rectangular parallelepiped resonance	Ambient	300–1100 300–700	13 (for *a*, *V*) 9 (for *c*)

'Ndata' is the number of data from each source used in the refinement of EoS parameters. This data is available in the Supplementary materials and at http://www.rossangel.net as .dat text files that can be read by the *EosFit* suite of programs.

experiments cannot be excluded. This deviation of properties cannot be described by a simple EoS, and therefore we only used data up to 1100 K in our analysis. The dataset used to determine the elastic parameters of rutile therefore consists of 111 data (Table 1), made up of 17 direct measurements of elastic moduli, 12 direct measurements of dimensional changes with temperature by interferometry and 82 determinations of unit-cell parameters by diffraction.

Equation of State analysis

All fits of elastic parameters were performed with the *EosFit7c* program (Angel *et al.*, 2014) following the approach of Milani *et al.* (2017) to perform simultaneous fits of elastic moduli and cell parameters. Initial fits of the cell parameters with temperature yield values of the linear thermal expansion coefficients of $\alpha_1 = \alpha_2 \sim 0.77 \times 10^{-5} \mathrm{K}^{-1}$ and $\alpha_3 \sim 0.99 \times 10^{-5} \mathrm{K}^{-1}$. The room-temperature elastic moduli (e.g. Isaak *et al.*, 1998) give values of the adiabatic linear moduli of $M_{1SR} = M_{2SR} \sim 506$ GPa and $M_{3SR} \sim 1149$ GPa. The *c* axis is therefore more than twice as stiff as the *a* axis, but it also has a significantly higher thermal expansion coefficient. This has an important consequence for the types of EoS that can be used to fit the data for rutile. The gradient of a line of constant unit-cell parameter *a* in *P*–*T* space is defined by $\left(\frac{\partial P}{\partial T}\right)_a = \alpha_1 M_{1TR}$. An equivalent expression applies for *c*. We do not have direct measurements of the isothermal moduli M_{1TR} and M_{3TR} but they do not differ by more than 2% from the adiabatic values, as we confirm in our analysis described later. Therefore, for initial analysis we can determine the approximate slopes of lines of constant *a* and *c* cell parameters at room conditions from the adiabatic moduli as $\left(\frac{\partial P}{\partial T}\right)_a \sim 3.9$ MPa K^{-1} and $\left(\frac{\partial P}{\partial T}\right)_c \sim 11.3$ MPa K^{-1}. These values differ by a factor of 3, implying that lines of constant *a* and *c* diverge rapidly in *P*–*T* space (Fig. 3*a*). Neither do these lines follow the isochor through room conditions, whose slope is given by the product of the volume thermal expansion coefficient and the isothermal Reuss bulk modulus, $\left(\frac{\partial P}{\partial T}\right)_V = \alpha_V K_{TR}$. Therefore, while along an isochor of rutile the volume does not change, the *a* and *c* cell parameters

change significantly (Fig. 3*b*), generating significant unit cell strains (in Voigt notation) $\varepsilon_1 = \frac{\Delta a}{a} = \varepsilon_2 = \frac{\Delta b}{b}$ and $\varepsilon_3 = \frac{\Delta c}{c}$. Along an isochor the linear strains sum to zero because:

$$\varepsilon_V = \frac{\Delta V}{V} = \varepsilon_1 + \varepsilon_2 + \varepsilon_3 \tag{1}$$

The frequencies of vibrational modes are primarily dependent upon the strains applied to the unit cell (e.g. Grüneisen, 1926; Barron *et al.*, 1980; Angel *et al.*, 2019). Therefore, in rutile the phonon mode frequencies must change along isochors. This violates the fundamental assumption of the quasi-harmonic approximation (QHA) to the thermodynamics of solids (e.g. Anderson, 1995) which underlies the derivation of thermal-pressure EoS such as Mie-Grüneisen-Debye (MGD) or the simplified thermal-pressure model of Holland and Powell (2011).

A simple consequence is that such QHA-based EoS cannot simultaneously fit all of the volume and elasticity data of rutile. For example, if the pressure derivative of the bulk modulus $\left(\frac{\partial K}{\partial P}\right)_{T=298K} = K'_0$ is held to the value of 6.92 (average of values from Manghnani, 1969; Fritz, 1974) determined by direct measurements of the elasticity of rutile, then refinement of the other parameters of an MGD EoS to the selected data for rutile do not allow the measured variation of K_{SR} with temperature (Isaak *et al.*, 1998) to be fit (Fig. 4). Instead, a value of $K'_0 \approx 9$ is required to fit the variation of K_{SR} with temperature, but such a high value is incompatible with the high-pressure measurements of the volume and elasticity (Manghnani, 1969; Fritz, 1974). This confirms the conclusion of Lan *et al.* (2015) that the QHA does not apply to rutile. Therefore, to fit the data of rutile we have used an 'isothermal' type of EoS in which there are no underlying assumptions of quasi-harmonic behaviour (Angel *et al.*, 2018). In an 'isothermal' EoS, the volume at *P* and *T* is obtained by first calculating the volume thermal expansion at room pressure to the *T* of interest. Then an isothermal EoS is used to calculate the isothermal compression at the temperature *T* from room pressure to the final pressure. This requires that the temperature variation of K_{TR} and K'_{TR} must be described by additional parameters (Angel *et al.*, 2018). The disadvantage of this approach compared to thermal-pressure EoS based on QHA is that it requires more parameters, and therefore other constraints
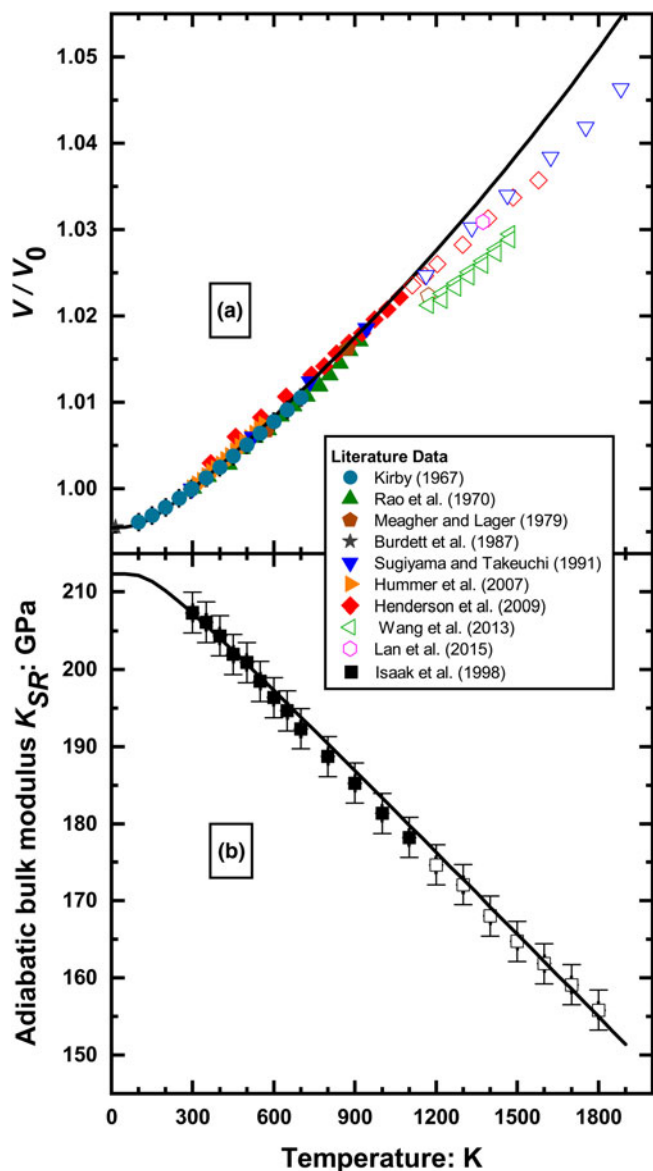
Fig. 2. (a) *T–V* data of rutile taken from the literature; (*b*) the variation of the adiabatic Reuss bulk modulus determined by Isaak *et al.* (1998), showing the decrease in the temperature variation of the bulk modulus above 1100 K. The open symbols are the data excluded from the current analysis. The full symbols are the selected data fitted with the final EoS (solid lines) with the parameters given in Table 2.

or restraints on the EoS parameters must be introduced when, as is the case for rutile, the available data are insufficient to determine all of the parameter values independently. We discuss the appropriate constraints as we present the results of our analysis below.

Volume Equation of State

As noted above, the direct measurements of the elastic moduli of rutile at high pressures show that K'_0 is significantly higher than 4, so we use a Birch-Murnaghan 3rd-order EoS (Birch, 1947) to describe the compressional behaviour in which K_{TR0} and K'_{TR0} are the parameters to be determined. For thermal expansion at room pressure we use the equation developed by Kroll *et al.* (2012) as a version of the Holland and Powell (2011) model, which describes the thermal expansion in terms of an Einstein
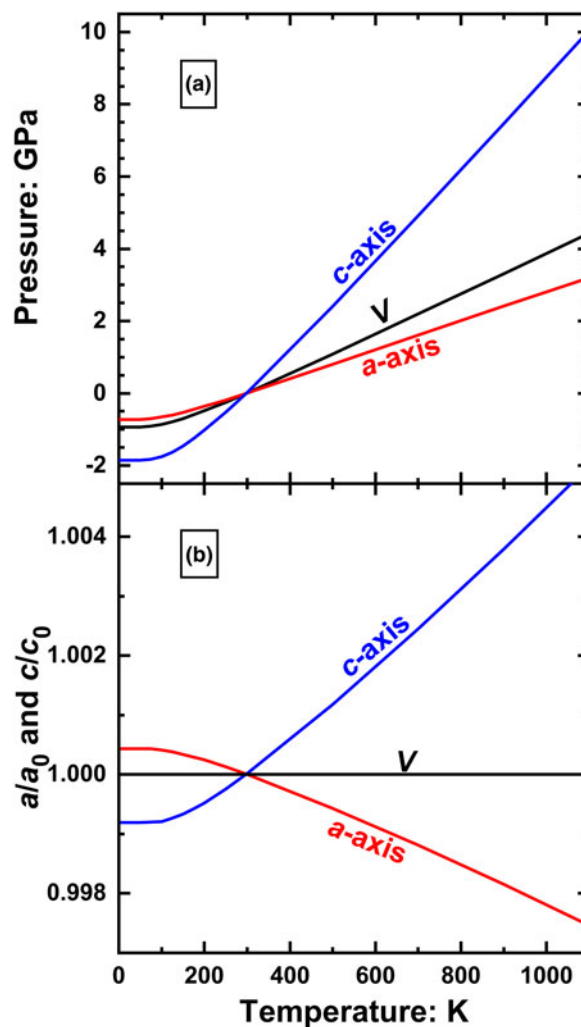

Fig. 3. (*a*) The lines of constant *a* and *c* of rutile in *P–T* space calculated from the final refined elastic parameters (Table 2) deviate significantly from the isochor that passes through room conditions; (*b*) as a consequence, the unit cell parameters of rutile change significantly along the isochor.

oscillator. But we explicitly use the Anderson-Grüneisen parameter δ_T (Anderson 1995) in place of $(1 + K'_T)$. This approach separates the thermal and baric parts of the EoS (Angel *et al.*, 2018) while maintaining a reasonable physical basis in the Einstein oscillator model behind the thermal expansion model. The separation of variables (Angel *et al.*, 2018) allows both the room-*T* high-pressure data and the variation of the bulk modulus with temperature to be fitted. We also use δ_T to define the temperature variation of the bulk modulus in a way (Anderson, 1995; Hellfrich and Connolly, 2009; Angel *et al.*, 2018) that is thermodynamically valid:

$$K_{TR}(T, P = 0) = K_{TR0} \left(\frac{V_0}{V(T)} \right)^{\delta_T} \tag{2}$$

There are no data available for rutile to constrain the temperature variation of K', so we have to assume that $(\partial K'_{TR}/\partial T)_P = 0$. The thermal effects in the EoS are therefore described by the thermal expansion coefficient at room conditions α_{V0}, the Einstein temperature θ_E (Holland and Powell, 2011) and the Anderson-Grüneisen parameter δ_T. The isotropic thermal Grüneisen
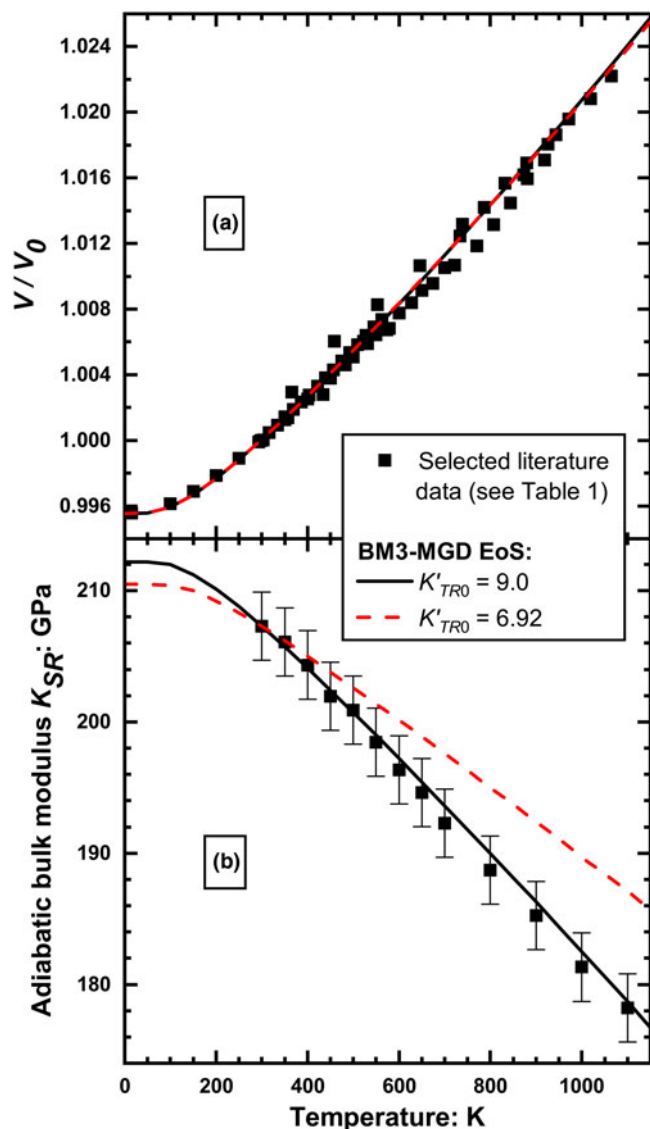
Fig. 4. The variation with temperature of (a) volume and (b) adiabatic Reuss bulk modulus of rutile. The volume variation is well-reproduced by an MGD thermal-pressure EoS with a wide range of K'_{TR0}. The bulk modulus data can only be modelled with $K'_{TR0} \approx 9$, a value that is incompatible with the high-pressure volume and elasticity data.

parameter γ_V (Anderson, 1995) is needed to relate the isothermal bulk moduli used to describe the volume variation with pressure, to the adiabatic bulk moduli measured in ultrasonic resonance (Isaak et al., 1998) and wave velocity experiments (Manghnani, 1969):

$$K_S = (1 + \alpha_V \gamma_V T)K_T \qquad (3)$$

The value of γ_V for rutile is not known exactly but appears to lie in the range of 1.2 to 1.6 at room conditions, and to either increase or decrease to 1.6 or 1.4 at 1100 K (see Isaak et al., 1998, fig. 9). Test fits of isothermal-type EoS to the selected data for rutile indicate that the particular value chosen for γ_V within this range has no significant influence on the refined parameters of the EoS or the quality of fit to the data. We therefore used an average value of $\gamma_V = 1.4$ and assumed that it does not

vary over the temperature interval 0–1100 K. Because rutile is so stiff, it is also necessary to over-weight (by artificially reducing its uncertainty) the experimental datum for K_{SR} at room conditions in order to stabilise the refinement. With these constraints the final refined EoS parameters reported in Table 2 are obtained, which clearly fit all of the selected experimental data within the experimental uncertainties (Figs 1, 2). But whether these EoS parameters correctly predict the volume of rutile outside the range of the underlying data (to 7.3 GPa and 1100 K) is not known. The values of δ_T and K'_{TR} are significantly different from one another, which indicates that the bulk modulus variation along an isochor, $\left(\frac{\partial K_{TR}}{\partial T}\right)_V = \alpha_V K_{TR}(K'_{TR} - \delta_T)$, is –0.004(3) GPa K^{-1}, a value similar to that estimated for olivine (e.g. Anderson et al., 1992; Angel et al., 2018).

Cell parameters

As for the volume, the values of the anisotropic thermal Grüneisen parameters cannot be refined and must be fixed to values determined independently. For the principal axes of compression the thermodynamically-correct expression that relates the corresponding adiabatic and isothermal linear moduli M_{iS} and M_{iT} can be derived (Nye, 1957; Barron et al., 1980; Milani et al., 2017) from the relationship between the adiabatic and isothermal elastic compliance tensors as:

$$M_{iS} = \left(1 + \alpha_i \gamma_V T \frac{M_{iS}}{K_S}\right)M_{iT} \qquad (4)$$

However, the bulk modulus K_S required for this conversion of the linear moduli is not always available when fits of unit-cell parameters are performed. Within the EosFit7c program anisotropic thermal Grüneisen parameters γ_i are therefore used in an equation analogous to (3):

$$M_{iS} = (1 + 3\alpha_i \gamma_i T)M_{iT} \qquad (5)$$

The values of the anisotropic thermal Grüneisen parameters used in EosFit7c are then given by:

$$\gamma_i = \frac{1}{3}\frac{M_{iS}}{K_S}\gamma_V \qquad (6)$$

Note that for materials such as rutile with significant elastic anisotropy, $\gamma_i \neq \gamma_V$. The other EoS parameters are not especially sensitive to the values of γ_i, which were therefore obtained (Table 2) from γ_V by using the values of the elastic moduli determined at room temperature (Isaak et al., 1998).

The variation of the unit-cell parameters of a crystal with pressure is always proportionally smaller than that of the volume. For a stiff material such as rutile there is too little variation of the a and c unit-cell parameters over the accessible pressure range to allow simultaneous refinement of both the linear moduli M_{iTR} and their pressure derivatives M'_{iTR}. We therefore constrained some of these parameters to values that are consistent with both the data for the a and c axes and the corresponding parameters for the volume, and we confirmed after fitting that the remaining refined parameters for the a and c unit-cell parameters were consistent with the volume parameters. Because the volume strain of the crystal induced by a change in T or P is given by the sum of

Table 2. Best-fit elastic parameters for rutile.

	Volume		a axis	c axis
K_{TR0}: GPa	205.14(15)	M_{iTR0}: GPa	502.3(4)	1123.0 fixed
K_{SR0}: GPa	207.30(14)	M_{iSR0}: GPa	506.1(4)	1149.1
K'_{TR0}	6.9(4)	M'_{iTR0}	18.8 fixed	19.4 fixed
K''_{TR0}: GPa^{-1}	–0.075 implied value	M''_{iTR0}: GPa^{-1}	–0.202 implied value	–0.100 implied value
α_{V0}: K^{-1}	2.526(16) x 10^{-5}	α_{i0}: K^{-1}	0.769(4) x 10^{-5}	0.998(7) x 10^{-5}
θ_E: K	328(12)	θ_E: K	307(7)	391(9)
δ_T	7.6(6)	δ_T	9.0(4)	5.8(6)
δ'	0.0 fixed	δ'	0.0 fixed	0.0 fixed
γ_0	1.4 fixed	γ_{i0}	1.1 fixed	2.6 fixed
q	0.0 fixed	q	0.0 fixed	0.0 fixed
Ndata	111		107	103

Parameters for a Birch–Murnaghan 3rd-order EoS, combined with the Holland and Powell (2011) thermal expansion model as modified following Kroll *et al.* (2012) and the temperature variation of bulk modulus after Hellfrich and Connolly (2009). For a full definition of these parameters, see Angel *et al.* (2018). 'Ndata' is the number of data used in the refinement of EoS parameters. These parameters are available in the Supplementary materials and at http://www.rossangel.net as .eos files that can be used in the *EosFit* suite of programs.

the linear strains of the unit-cell parameters (equation 1), it follows that the axial thermal expansion and compressibilities sum to the corresponding quantities for the volume:

$$\alpha_V = \frac{1}{V}\left(\frac{\partial V}{\partial T}\right)_P = \alpha_1 + \alpha_2 + \alpha_3$$
$$\beta_V = \frac{1}{V}\left(\frac{\partial V}{\partial P}\right)_T = \beta_1 + \beta_2 + \beta_3. \quad (7)$$

Because the volume compressibility is the inverse of the isothermal Reuss bulk modulus, $K_{TR} = -V\left(\frac{\partial P}{\partial V}\right)_T$, and the linear compressibilities are the inverse of the corresponding isothermal Reuss linear moduli, $M_{iTR} = -l_i\left(\frac{\partial P}{\partial l_i}\right)_T$, the relationship between these moduli must always be:

$$K_{TR} = (M_{1TR}^{-1} + M_{2TR}^{-1} + M_{3TR}^{-1})^{-1} \quad (8)$$

Differentiation of (8) gives the relationship between the first pressure derivatives of the moduli:

$$K'_{TR} = K_{TR}^2 \sum_{i=1}^{3} \frac{M'_{iTR}}{M_{iTR}^2} \quad (9)$$

In the fits to the data, the values of M'_{iTR} (Table 2) were taken from Fritz (1974) with a slight adjustment within the reported experimental uncertainties to ensure that they conform to equation 9. In addition, the linear modulus of the *c* axis, M_{3TR0}, cannot be refined simultaneously with the value of δ_T and it was therefore fixed to a value consistent with the experimental determinations of M_{3SR} at room temperature (Isaak *et al.*, 1998) and the calculated value of γ_3. The values of the remaining parameters obtained by refinement are reported in Table 2. They fulfil the consistency requirements given in equations 7, 8, and 9, and reproduce the experimental data within their uncertainties.

Conclusions

We have demonstrated that for stiff minerals it is possible to obtain more reliable EoS parameters by fitting experimental elastic moduli and cell parameter data simultaneously. Of particular importance, in the absence of data collected at simultaneous

high *T* and *P*, is the use of high-temperature measurements of the elastic moduli to constrain the *P–T* 'cross-terms' in the EoS. Without such data, it is not possible to determine whether the quasi-harmonic approximation is valid or not for the mineral, as we have done in Fig. 4. For materials such as rutile in which $\alpha_i M_{iTR}$ varies strongly with direction in the crystal, EoS based on QHA are not only theoretically invalid but also cannot fit all of the available experimental data. The isothermal types of EoS do not suffer from this theoretical problem, but they involve more parameters than can be determined independently from the experimental data for stiff materials such as rutile. Applying the requirements for consistency between linear and volume parameters of the EoS can help overcome this issue in a thermodynamically-consistent manner. The resulting elastic parameters for the volume and unit-cell parameters of rutile (Table 2) are also available as .eos files in the Supplementary materials (see below) for this paper and from the website http://www.rossangel.net for use in the *EosFit7* suite of programs.

As noted above, rutile is a very common inclusion in metamorphic garnets. Minerals trapped as inclusions within other host minerals can exhibit residual pressures when measured at room conditions because of the differences between the thermo-elastic properties of the host and inclusion phases. This residual or remnant pressure can be measured by a variety of techniques such as diffraction or spectroscopy (e.g. Kohn, 2014; Murri *et al.*, 2018; Angel *et al.*, 2019), and with knowledge of the EoS of both the host and inclusion phases the *P* and *T* of inclusion entrapment can be inferred (Rosenfeld and Chase, 1961). To understand the development of inclusion pressures Rosenfeld and Chase (1961) introduced the thermodynamic concept of an 'isomeke' (first named as such by Adams *et al.*, 1975). The isomeke is the only path in *P–T* space along which no residual pressures would be developed in the inclusion after entrapment. The slope of an isomeke is $\left(\frac{\partial P}{\partial T}\right)_{V_I - V_H} = \frac{\alpha_I - \alpha_H}{\beta_I - \beta_H}$ where the subscript '*I*' indicates the inclusion and the subscript '*H*' the host mineral, α is the volume thermal expansion coefficient and β is the volume compressibility (e.g. Rosenfeld and Chase, 1961; Angel *et al.*, 2015). Rutile (Table 2) is stiffer than pyrope and has a similar thermal expansion coefficient to that of pyrope (Milani *et al.* 2015), which means that $\beta_I < \beta_H$ and $\alpha_I \simeq \alpha_H$. Therefore, the isomekes of rutile trapped in pyrope are almost flat, as shown in Fig. 5a; in particular, the isomeke passing through room conditions has $\partial P/\partial T \simeq 0$ at temperatures below ~600 K and a negative $\partial P/\partial T$ at higher temperatures. In fact,
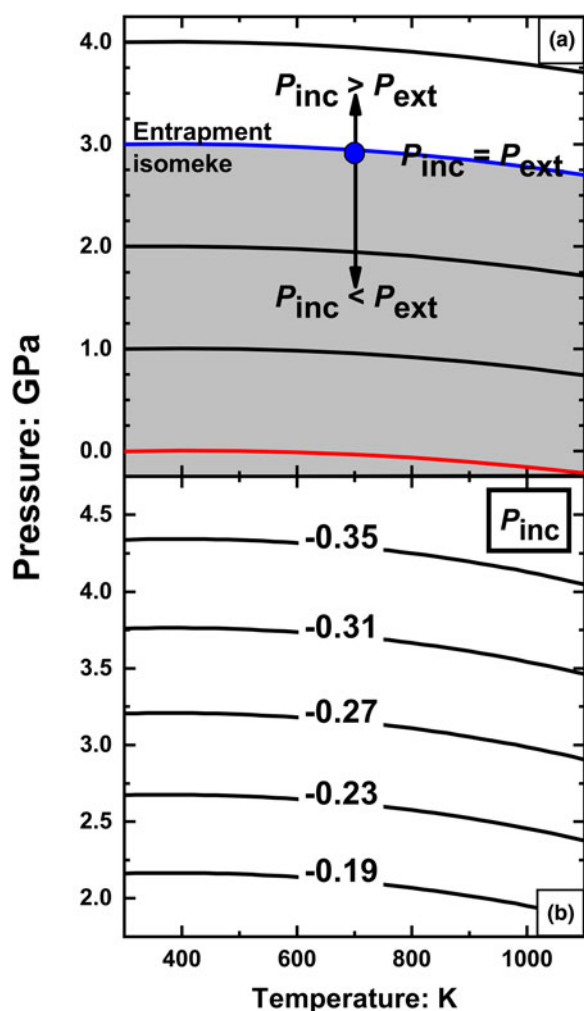
Fig. 5. (*a*) Isomekes for rutile and pyrope. Consider a rutile inclusion trapped in pyrope at 700 K and 2.95 GPa (blue spot). If the external pressure is raised above the entrapment isomeke (blue line) the inclusion will have a higher pressure than the external pressure. At external pressures below the entrapment isomeke, the inclusion pressure is lower than the external pressure. The red line is the isomeke passing through room conditions; in order for an inclusion measured at room conditions to exhibit a positive residual inclusion pressure it must be trapped below the red isomeke; (*b*) Entrapment isomekes showing the residual pressures P_{inc} (GPa) in an inclusion measured at room conditions as a function of the entrapment P and T.

$\beta_I - \beta_H$ is always negative over the P–T range shown in Fig. 5 but α_I becomes larger than α_H at higher temperatures leading to a negative $\partial P/\partial T$.

When the host-inclusion system leaves the isomeke, a residual pressure is developed in the inclusion. This can be most easily understood for a small isothermal change in the external pressure, P_{ext}, applied to the host. By definition of the isothermal bulk modulus of the host, the change in volume of the inclusion cavity will be $\dfrac{\Delta V}{V} = \dfrac{-\Delta P_{ext}}{K_H}$. This volume change applied to the inclusion changes its pressure by $\Delta P_{inc} = \dfrac{K_I}{K_H}\Delta P_{ext}$ (Angel *et al.*, 2017; Ferrero and Angel, 2018). For a stiff inclusion trapped in a softer host mineral, like the case of rutile trapped in pyrope, the change in the inclusion pressure ΔP_{inc} will always be greater than the change in external pressure ΔP_{ext}. Therefore, when the system is taken to a P and T above the entrapment isomeke, the residual pressure (P_{inc}) will be higher than the external pressure (P_{ext}).

On the contrary, when the system is taken to lower external P than the entrapment isomeke, P_{inc} will be less than P_{ext} (Fig. 5*a*). Therefore, rutile inclusions will exhibit positive P_{inc} at room conditions only if room conditions lie above the entrapment isomeke. The isomeke through room conditions (Fig. 5*a*) thus divides P–T space in two areas: rutile inclusions trapped below this isomeke will exhibit positive P_{inc} when measured at room conditions, whereas rutile inclusions trapped above this isomeke will exhibit negative P_{inc}. This means that rutile inclusions trapped in pyrope from ultra-high-pressure metamorphic rocks should always exhibit negative residual pressures. The calculated P_{inc} as a function of entrapment conditions are shown as contours in Fig. 5*b*. A negative value of P_{inc} represents an expansion of the inclusion crystal relative to a free crystal of rutile at room conditions. Such expansion could only occur if rutile inclusion crystals are strongly bonded to the garnet host at the host/inclusion interface. If such bonding does not occur, then rutile inclusions will be free to contract back to the volume of a free crystal at room conditions, leaving a void space between the inclusion crystal and the host crystal. If that occurs, the inclusions will exhibit a pressure equal to ambient P, independent of the conditions of entrapment. Rutile inclusions in pyrope garnets from Dora Maira massif measured with Raman spectroscopy (N. Campomenosi, 2018, pers. comm.) exhibit zero residual pressure (within the measurement uncertainties), thus confirming this analysis and that the rutile inclusion crystals become mechanically detached from the garnet host. The same conclusion is obtained even if the EoS for rutile of Holland and Powell (2011) is used. It has a much lower volume thermal expansion coefficient and a stiffer bulk modulus that do not reproduce the experimental data (Tables 1) as well as the EoS given in Table 2. The rutile-pyrope isomekes calculated with it therefore have slopes more positive than those shown in Fig. 5*a*, but the bulk modulus contrast between rutile and garnet ensures that it still predicts that the final P_{inc} will be negative for rutile inclusions entrapped at metamorphic conditions. Rutile trapped in other garnet compositions should also show negative or zero residual pressures because all garnets in metamorphic rocks are significantly less stiff than rutile (Milani *et al.*, 2015; Milani *et al.*, 2017).

The determination of the variation of the unit-cell parameters of rutile (Table 2) also allows us to calculate the residual unit-cell strains expected for rutile inclusions in garnets. These calculations show that at room conditions the *c* axis of a rutile inclusion will be stretched compared to the *c* axis of a free crystal of rutile (i.e. positive strain) whereas the *a* axis will exhibit a compressive strain (i.e. negative strain) but these strains always result in a positive volume strain and thus negative P_{inc}. All of these observations lead to the conclusion that rutile is not suitable for elastic geobarometry when it is trapped in garnet. This contrasts with the behaviour of zircon inclusions trapped in garnet which exhibit positive P_{inc} when measured at room conditions (Campomenosi *et al.*, 2018; Stangarone *et al.*, 2019) even though zircon (e.g. Van Westrenen *et al.*, 2004; Zaffiro *et al.*, 2018), like rutile, is stiffer than garnet. In the case of zircon however, the contrast in bulk modulus with the garnets is compensated by the substantially lower thermal expansion coefficient of zircon. Therefore, stiff inclusions trapped in softer host minerals are suitable for elastic geobarometry only when α_V of the inclusion is significantly lower than the α_V of the host, which is not the case of rutile inclusions trapped in garnet hosts.

Author ORCIDs. ⓘ Ross J. Angel, 0000-0003-0861-398X

References

Adams H.G., Cohen L.H. and Rosenfeld J.L. (1975) Solid inclusion piezother-mometry I: comparison dilatometry. *American Mineralogist*, **60**, 574–583.

Al-Khatatbeh Y., Lee K.K. and Kiefer B. (2009) High-pressure behavior of TiO₂ as determined by experiment and theory. *Physical Review B*, **79**, 134114.

Al'tshuler L.V., Podurets M.A., Simakov G.V. and Trunin R.F. (1973) High-density forms of fluorite and rutile. *Soviet Physics Solid State*, **15**, 969–971.

Anderson O.L. (1995) *Equations of State of Solids for Geophysics and Ceramic Science*. Oxford University Press, Oxford, UK, 432 pp.

Anderson O.L., Isaak D. and Oda H. (1992) High-temperature elastic constant data on minerals relevant to geophysics. *Reviews of Geophysics*, **30**, 57–90.

Angel R.J., Gonzalez-Platas J. and Alvaro M. (2014) EosFit7c and a Fortran module (library) for equation of state calculations. *Zeitschrift für Kristallographie*, **229**, 405–419.

Angel R.J., Nimis P., Mazzucchelli M.L., Alvaro M. and Nestola F. (2015) How large are departures from lithostatic pressure? Constraints from host-inclusion elasticity. *Journal of Metamorphic Geology*, **33**, 801–813.

Angel R.J., Mazzucchelli M.L., Alvaro M. and Nestola F. (2017) EosFit-Pinc: A simple GUI for host-inclusion elastic thermobarometry. *American Mineralogist*, **102**, 1957–1960.

Angel R.J., Alvaro M. and Nestola F. (2018) 40 years of mineral elasticity: a critical review and a new parameterisation of Equations of State for mantle olivines and diamond inclusions. *Physics and Chemistry of Minerals*, **45**, 95–113.

Angel R.J., Murri M., Mihailova B. and Alvaro M. (2019) Stress, strain and Raman shifts. *Zeitschrift für Kristallographie*, **234**, 129–140.

Arashi H. (1992) Raman spectroscopic study of the pressure-induced phase transition in TiO₂. *Journal of Physics and Chemistry of Solids*, **53**, 355–359.

Barron T.H.K., Collins J.G. and White G.K. (1980) Thermal expansion of solids at low temperatures. *Advances in Physics*, **29**, 609–730.

Birch F. (1947) Finite elastic strain of cubic crystals. *Physical Review*, **71**, 809–824.

Burdett J.K., Hughbanks T., Miller G.J., Richardson Jr J.W. and Smith J.V. (1987) Structural-electronic relationships in inorganic solids: powder neutron diffraction studies of the rutile and anatase polymorphs of titanium dioxide at 15 and 295 K. *Journal of the American Chemical Society*, **109**, 3639–3646.

Campomenosi N., Mazzucchelli M.L., Mihailova B., Scambelluri M., Angel R.J., Nestola F., Reali A. and Alvaro M. (2018) How geometry and anisotropy affect residual strain in host inclusion system: coupling experimental and numerical approaches. *American Mineralogist*, **103**, 2032–2035.

Dubrovinskaia N.A., Dubrovinsky L.S., Ahuja R., Prokopenko V.B., Dmitriev V., Weber H.-P., Osorio-Guillen J.M. and Johansson B. (2001) Experimental and theoretical identification of a new high-pressure TiO₂ polymorph. *Physical Review Letters*, **87**, 275501.

Ferrero S. and Angel R.J. (2018) Micropetrology: are inclusions grains of truth? *Journal of Petrology*, **59**, 1671–1700.

Fritz I.J. (1974) Pressure and temperature dependences of the elastic properties of rutile (TiO₂). *Journal of the Physics and Chemistry of Solids*, **35**, 817–826.

Gerward L. and Staun Olsen J. (1997) Post-rutile high-pressure phases in TiO₂. *Journal of Applied Crystallography*, **30**, 259–264.

Grüneisen E. (1926) Zustand des festen Körpers. *Handbuch der Physik*, **1**, 1–52.

Hazen R.M. and Finger L.W. (1981) Bulk moduli and high-pressure crystal structures of rutile-type compounds. *Journal of Physics and Chemistry of Solids*, **42**, 143–151.

Hellfrich G. and Connolly J.A.D. (2009) Physical contradictions and remedies using simple polythermal equations of state. *American Mineralogist*, **94**, 1616–1619.

Henderson C.M.B., Knight K.S. and Lennie A.R. (2009) Temperature dependence of rutile (TiO₂) and geikielite (MgTiO₃) structures determined using neutron powder diffraction. *The Open Mineralogy Journal*, **3**, 1–11.

Holland T.J.B. and Powell R. (2011) An improved and extended internally consistent thermodynamic dataset for phases of petrological interest, involving a new equation of state for solids. *Journal of Metamorphic Geology*, **29**, 333–383.

Hummer D.R., Heaney P.J. and Post J.E. (2007) Thermal expansion of anatase and rutile between 300 and 575 K using synchrotron powder X-ray diffraction. *Powder Diffraction*, **22**, 352–357.

Isaak D.G., Carnes J.D., Anderson O.L., Cynn H. and Hake E. (1998) Elasticity of TiO₂ rutile to 1800 K. *Physics and Chemistry of Minerals*, **26**, 31–43.

Kirby R.K. (1967) Thermal expansion of rutile from 100 to 700 K. Journal of Research of the National Bureau of Standards – A. *Physics and Chemistry*, **71A**, 363–369.

Kohn M.J. (2014) "Thermoba-Raman-try": Calibration of spectroscopic barometers and thermometers for mineral inclusions. *Earth and Planetary Science Letters*, **388**, 187–196.

Kojitani H., Yamazaki M., Kojima M., Inaguma Y., Mori D. and Akaogi M. (2018) Thermodynamic investigation of the phase equilibrium boundary between TiO₂ rutile and its α-PbO₂-type high-pressure polymorph. *Physics and Chemistry of Minerals*, **45**, 963–980.

Kroll H., Kirfel A., Heinemann R. and Barbier B. (2012) Volume thermal expansion and related thermophysical parameters in the Mg,Fe olivine solid-solution series. *European Journal of Mineralogy*, **24**, 935–956.

Kudoh Y. and Takeda H. (1986) Single crystal X-ray diffraction study on the bond compressibility of fayalite, Fe₂SiO₄ and rutile, TiO₂ under high pressure. *Physica B*, **139 & 140**, 333–336.

Lan T., Li C.W., Hellman O., Kim D.S., Munoz J.A., Smith H., Abernathy D.L. and Fultz B. (2015) Phonon quarticity induced by changes in phonon-tracked hybridization during lattice expansion and its stabilization of rutile TiO₂. *Physical Review B*, **92**, 054304.

Mammone J.F., Sharma S.K. and Nicol M. (1980) Raman study of rutile (TiO₂) at high pressures. *Solid State Communications*, **34**, 799–802.

Manghnani M.H. (1969) Elastic constants of single-crystal rutile under pressures to 7.5 kilobars. *Journal of Geophysical Research*, **74**, 4317–4328.

Manghnani M.H., Fisher E.S. and Brower Jr W.S. (1972) Temperature dependence of the elastic constants of single-crystal rutile between 4 and 583 K. *Journal of Physics and Chemistry of Solids*, **33**, 2149–2159.

McQueen R.G., Jamieson J.C. and Marsh S.P. (1967) Shock-wave compression and X-ray studies of titanium dioxide. *Science*, **155**, 1401–1404.

Meagher E.P. and Lager G.A. (1979) Polyhedral thermal expansion in the TiO₂ polymorphs; refinement of the crystal structures of rutile and brookite at high temperature. *The Canadian Mineralogist*, **17**, 77–85.

Mei Z.G., Wang Y., Shang S. and Liu Z.K. (2014) First-principles study of the mechanical properties and phase stability of TiO₂. *Computational Materials Science*, **83**, 114–119.

Meinhold G. (2010) Rutile and its applications in earth sciences. *Earth-Science Reviews*, **102**, 1–28.

Milani S., Nestola F., Alvaro M., Pasqual D., Mazzucchelli M.L., Domeneghetti M.C. and Geiger C. (2015) Diamond–garnet geobarometry: The role of garnet compressibility and expansivity. *Lithos*, **227**, 140–147.

Milani S., Angel R.J., Scandolo L., Mazzucchelli M.L., Boffa-Ballaran T., Klemme S., Domeneghetti M.C., Miletich R., Scheidl K.S., Derzsi M., Tokar K., Prencipe M., Alvaro M. and Nestola F. (2017) Thermo-elastic behaviour of grossular garnets at high pressures and temperatures. *American Mineralogist*, **102**, 851–859.

Ming L.C. and Manghnani M.H. (1979) Isothermal compression of TiO₂ (rutile) under hydrostatic pressure to 106 kbar. *Journal of Geophysical Research*, **84**, 4777–4779.

Murri M., Mazzucchelli M.L., Campomenosi N., Korsakov A.V., Prencipe M., Mihailova B., Scambelluri M., Angel R.J. and Alvaro M. (2018) Raman elastic geobarometry for anisotropic mineral inclusions. *American Mineralogist*, **103**, 1869–1872.

Nicol M. and Fong M.Y. (1971) Raman spectrum and polymorphism of titanium dioxide at high pressures. *Journal of Chemical Physics*, **54**, 3167–3170.

Nye J.F. (1957) *Physical Properties of Crystals*. Oxford University Press, Oxford, 329 pp.

Rao K.K., Naidu S.N. and Iyengar L. (1970) Thermal expansion of rutile and anatase. *Journal of the American Ceramic Society*, **53**, 124–126.

Rosenfeld J.L. and Chase A.B. (1961) Pressure and temperature of crystallization from elastic effects around solid inclusion minerals? *American Journal of Science*, **259**, 519–541.

Sato Y. (1977) Equation of state of mantle minerals determined through high-pressure X-ray study. Pp 307–323 in: *High-Pressure Research: Applications in Geophysics* (M. H. Manghnani and S.-I. Akimoto, editors). American Geophysical Union, Washington DC.

Stangarone C., Alvaro M., Angel R., Prencipe M. and Mihailova B.D. (2019) Determination of the phonon-mode Grüneisen tensors of zircon by DFT simulations. *European Journal of Mineralogy*, doi: 10.1127/ejm/2019/0031-2851.

Sugiyama K. and Takeuchi Y. (1991) The crystal structure of rutile as a function of temperature up to 1600°C. *Zeitschrift für Kristallographie*, **194**, 305–313.

Syono Y., Kusaba K., Kikuchi M., Fukuoka K. and Goto T. (1987) Shock-induced phase transitions in rutile single crystal. Pp 385–392 in: *High-Pressure Research in Mineral Physics* (M. H. Manghnani and Y. Syono, editors). American Geophysical Union, Washington DC, USA.

Van Westrenen W., Frank M.R., Hanchar J.M., Fei Y.W., Finch R.J. and Zha C.S. (2004) In situ determination of the compressibility of synthetic pure zircon ($ZrSiO_4$) and the onset of the zircon-reidite phase transition. *American Mineralogist*, **89**, 197–203.

Wang L., Wang H.J. and Li T. (2013) In situ high temperature X-ray diffraction study of anatase and rutile. *Acta Physica Sinica*, **62**, 146402.

Zack T. and Kooijman E. (2017) Petrology and geochronology of rutile. pp. 433–467 in: *Petrochronology: Methods and Applications* (M. J. Kohn, M. Engi and P. Lanari, editors). Reviews in Mineralogy and Geochemistry, **83**. Mineralogical Society of America and the Geochemical Society, Chantilly, Virginia, USA.

Zaffiro G., Angel R.J., Alvaro M., Prencipe M. and Stangarone C. (2018) P-V-T-Ks Equations of State for zircon and rutile. *Geophysical Research Abstract*, **20**, 6952.

Zhang Y. (1998) Mechanical and phase equilibria in inclusion–host systems. *Earth and Planetary Science Letters*, **157**, 209–222.